



AALBORG UNIVERSITY
DENMARK

Aalborg Universitet

Autonomous Control of Distributed Generation and Storage to Coordinate P/Q Sharing in Islanded Microgrids

An Approach beyond Droop Control

Wu, Dan; Tang, Fen; Guerrero, Josep M.; Vasquez, Juan Carlos

Published in:

Proceedings of the 2014 IEEE International Energy Conference (ENERGYCON)

DOI (link to publication from Publisher):

[10.1109/ENERGYCON.2014.6850545](https://doi.org/10.1109/ENERGYCON.2014.6850545)

Publication date:

2014

Document Version

Early version, also known as pre-print

[Link to publication from Aalborg University](#)

Citation for published version (APA):

Wu, D., Tang, F., Guerrero, J. M., & Vasquez, J. C. (2014). Autonomous Control of Distributed Generation and Storage to Coordinate P/Q Sharing in Islanded Microgrids: An Approach beyond Droop Control. In *Proceedings of the 2014 IEEE International Energy Conference (ENERGYCON)* (pp. 983-988). IEEE Press. <https://doi.org/10.1109/ENERGYCON.2014.6850545>

General rights

Copyright and moral rights for the publications made accessible in the public portal are retained by the authors and/or other copyright owners and it is a condition of accessing publications that users recognise and abide by the legal requirements associated with these rights.

- Users may download and print one copy of any publication from the public portal for the purpose of private study or research.
- You may not further distribute the material or use it for any profit-making activity or commercial gain
- You may freely distribute the URL identifying the publication in the public portal -

Take down policy

If you believe that this document breaches copyright please contact us at vbn@aub.aau.dk providing details, and we will remove access to the work immediately and investigate your claim.

Autonomous Control of Distributed Generation and Storage to Coordinate P/Q Sharing in Islanded Microgrids – An Approach beyond Droop Control

Dan Wu[#], Fen Tang^{*}, Josep M. Guerrero[#], and Juan C. Vasquez[#]

[#] Institute of Energy Technology, Aalborg University, Denmark, Microgrids Research Programme www.microgrids.et.aau.dk
{dwu, joz, juq}@et.aau.dk

^{*} School of Electrical Engineering, Beijing Jiaotong University, P. R. China
ftang_nego@126.com

Abstract—In this paper, a decentralized control for coordinate both active and reactive powers is proposed for islanded microgrids. Compared with the conventional droop control strategies, the proposed control realizes decentralized power distribution among renewable energy sources (RES) and energy storage systems (ESS) according to the local source conditions. Based on bus-signaling method, the ESS is able to limit charging power by decreasing RES power generation automatically. As well, the reactive power coordinated control makes the RES units able to support reactive power in a decentralized way, which allows ESS providing for more active power availability. Moreover, the reactive power is distributed according to the apparent power capacity of each unit. The control strategy principle is simple and easy to implement without extra communication requirements. Real time hardware-in-the-loop results are presented to show the feasibility of proposed control strategy.

Keywords: AC Microgrids, Islanded mode, Coordinated control, Autonomous control.

I. INTRODUCTION

During last decade, microgrids are becoming more and more attractive due to the fast development of distributed generation (DG) technologies. Compared with the traditional power systems, integrating microgrids with DG bring the following advantages [1], [2]: (i) transmission losses can be reduced having power generation near to the consumption points; (ii) operation redundancy can be increased by increasing the number of DG units, thus reducing the chance in losing large amount of generation simultaneously; and (iii) higher power supply flexibility can be obtained since microgrid can supply local loads in both grid-connected or islanded situations.

From the control configuration viewpoint, the control algorithms can be classified as centralized or decentralized types [3]. The difference of these two approaches is whether there is a microgrid central controller (MGCC) to take decisions regarding power distribution. The centralized control can benefit from being more flexible to balance the power between generation and consumption and execute operating reserve to microgrids [4]. In this sense, communications are indispensable in centralized control [2], while when distributed units spatially allocated in wide range areas, it imposes high challenges in communication system

requirements. Hence, bus-signaling methods (BSM) [5], [6] or power line communications (PLC) [7], [8] constitute a potential way to overcome this limitation by using the power line as a communication carrier. However, PLC signals can be perturbed when supplying nonlinear loads or when the power stage presents unexpected resonances.

When applying decentralized control to microgrids with predefined droop characteristics in local units, it is possible to achieve active and reactive power distribution without using any MGCC [9], [10]. Nevertheless, real time active/reactive power coordination is hard to be implemented by using this method. Consequently, in our previous work [11] decentralized control based on BSM was proposed in order to achieve active power coordination among renewable energy sources (RES) and energy storage system (ESS) based on local source conditions.

In this paper, which is a continuation of our previous work, a decentralized control that integrates both active and reactive power coordination in islanded AC microgrids is proposed. By using this approach, the active power can be well coordinated based on the local ESS and RES conditions. Further, reactive power can also be well distributed among the microgrid units, based on the each capacity thus avoiding overloads.

II. PROPOSED DECENTRALIZED ACTIVE AND REACTIVE COORDINATED CONTROL STRATEGY

A typical microgrid configuration is shown in Fig. 1. The primary control of distributed ESS and RES units can be summarized as Fig. 2, According to the relation between frequency and active power, voltage amplitude and reactive power, the output characteristic of local control can be classified according to three types of curves: (i) ideal current control mode (CCM) with infinite slope value of P/ω and Q/V ; (ii) ideal voltage control mode (VCM) with zero slope; (iii) master /slave droop with constant slope value. Conventional control strategies use the three types of curves are applied on consistent active and reactive power regulation of ESS and RES units. Usually CCM (characteristic A) is applied on RES units to achieve constant power control, while VCM and droop control (characteristics B and C) are implemented

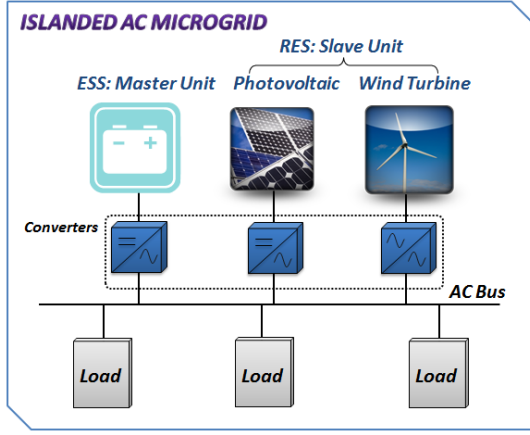


Fig. 1. A Typical configuration of a AC microgrid.

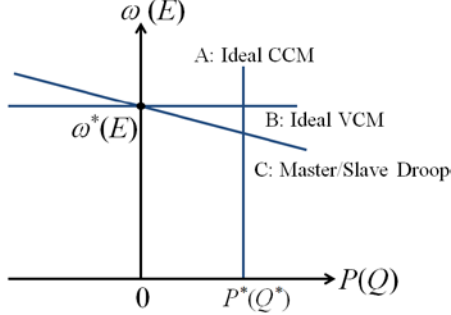


Fig. 2. Output characteristic of primary control with distributed units.

in ESS units to regulate the bus frequency/voltage and realize bidirectional power control. In the following Subsections, the three types of curves are applied to active and reactive power control in terms of different conditions of ESS and RES units.

A. Active Power Coordinated Control.

In case of adopting consistently curves A and B for active power control of ESS and RES respectively regardless state of charge (SoC) of the ESS unit, ESS overcharge or microgrid contingency situations may occur. Therefore, the active power control may utilize different output characteristic curves depending on SoC conditions, as shown in Fig. 3, which includes two ranges of coordinated control CR₁ and CR₂. In terms of ESS active power control, characteristic B is adopted in CR₁ when SoC below charging threshold SoC₁. In CR₂, i.e. when SoC is higher than SoC₁, a droop control based on BSM is applied to ESS. The ESS frequency deviation shown in Fig. 3(a) is based on the SoC value, but not on the ESS output active power as in conventional droop control shown in curve C. The objective of ESS primary control is to implement bus-signaling behavior that regulates bus frequency to inform other units the SoC condition. The initial point of ESS curve in CR₂ is (SoC₁, ω*), where ω* is the nominal angular frequency. The final point is set as (SoC_f, ω_m), where SoC_f is maximum SoC value which can be set as 100% by ignoring the SoC estimation error, and ω_m is maximum frequency value. It indicates that in the most serious case the bus frequency reaches the maximum value to define ESS is fully charged. Having these two points, the output characteristic curve of the ESS can be determined as

$$\begin{cases} \omega = \omega^* & \text{if } SoC \leq SoC_1 \\ \omega = \omega^* + m_E \cdot (SoC - SoC_1) & \text{if } SoC > SoC_1 \end{cases} \quad (0)$$

where the boost frequency coefficient m_E can be defined as

$$m_E = \frac{\omega_m - \omega^*}{SoC_f - SoC_1}. \quad (0)$$

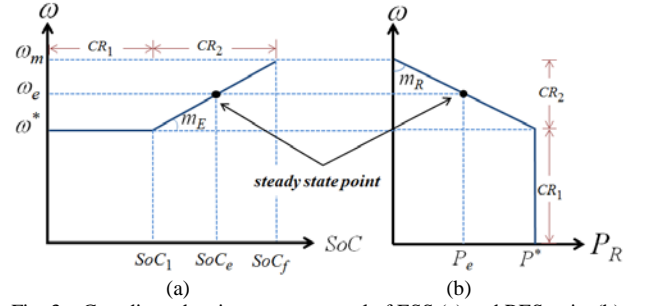


Fig. 3. Coordinated active power control of ESS (a) and RES units (b).

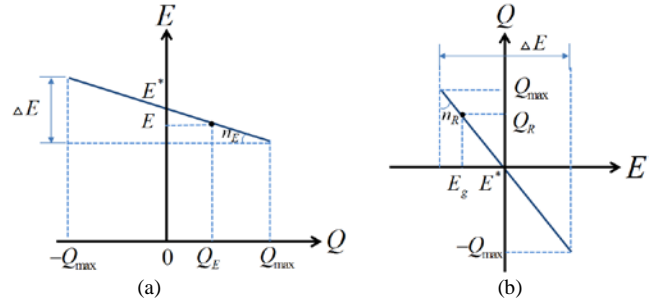


Fig. 4. Coordinated reactive power control of ESS (a) and RES units (b).

At the same time, the power generated by RES units should be coordinated with the bus frequency condition, as Fig. 3(b) shows. When the measured bus frequency is kept at nominal value in CR₁, each RES unit controls active power following curve A in Fig. 2 with a given constant reference value. When the bus frequency is continuously increasing following CR₂, it shows that charging power of ESS should be limited. In this case, each RES unit decreases generated power from given reference. The output characteristic can be classified as “slave droop” between output power and bus frequency in this range. In comparison to the conventional RES control in CR₁, the RES units obtain inertia performance based on the active power slave droop control in CR₂. The amount of RES active power reference deviation is calculated according to the measured bus frequency error.

Finally, when the power absorbed by the ESS is low enough to limit SoC at SoC_e, the bus frequency will be stable at ω_e, while power generated by RES units will be decreased automatically to P_e. In CR₂, the initial point of RES curve is (P*, ω*), where P* is active power reference of RES. The final point is set as (0, ω_m) which indicates in the most severe case that bus frequency reaches maximum value, the active power generation of RES will decrease to minimum value. With the defined two points, the coordinated curve of RES units is expressed as

$$\begin{cases} P_R = P^* & \text{if } \omega_{meas} \leq \omega^* \\ P_R = P^* - m_R \cdot (\omega_{meas} - \omega^*) & \text{if } \omega_{meas} > \omega^* \end{cases} \quad (0)$$

where P_R is the active power generated by RES unit, and ω_{meas} is the measured bus frequency with phase lock loop (PLL). The slave droop coefficient m_R of active power control can be designed as follows

$$m_R = \frac{P^*}{\omega_m - \omega^*}. \quad (0)$$

B. Reactive Power Coordinated Control.

In order to achieve autonomous reactive power sharing in VCM inverters, a conventional master droop control is often used as [9]

$$E = E^* - n_E Q_E \quad (0)$$

where E and E^* are the output voltage amplitude and its nominal values, Q_E is the output reactive power of ESS, and n_E is the droop coefficient. For the RES units operating in CCM, the slave droop can be applied to support reactive power as,

$$Q_R = \frac{1}{n_R} (E^* - E_g) \quad (0)$$

where E_g is the measured grid voltage amplitude and n_R is the droop coefficient. Supposing $E=E_g$ in an ideal measurement, we have the power distribution of the integrated ESS and RES units by combing (5) and (6),

$$Q_1 : Q_2 \cdots : Q_i = \frac{1}{n_1} : \frac{1}{n_2} \cdots : \frac{1}{n_i} \quad (0)$$

where Q_i is the output reactive power of each unit, n_i is the master/slave droop coefficients of reactive power. The master and slave droop characteristics for ESS and RES units are shown in Fig. 4.

Comparing the proposed approach with the conventional one that controls the reactive power to the given constant value, the coordinated reactive power control makes all the distributed units share the total reactive power of loads in a proportional way. According to (7), the reactive power distribution can be simply achieved by assigning proper sets of coefficients of n_i in a distributed way. When developing the reactive power coordinated control system, the reactive power coefficient n is designed as

$$n = \frac{\Delta E}{Q_{max}} \quad (0)$$

where Q_{max} is the maximum reactive power that the unit can provide ΔE is maximum bus voltage amplitude deviation, which should be designed within the limits fixed by standards. e.g. 10 % nominal voltage deviation according to EN 50160 [12]. In previous work, Q_{max} is set to the same value regardless the maximum apparent power S_{max} . However, reactive power control should take into account the active power flow as well thus adjusting Q_{max} . The active and reactive power distribution between two units is shown in Fig. 5. In Fig. 5, the two units provide for different active power, $P_1 < P_2$. Thus in case both have same maximum apparent power S_{max} , we have

$$Q_{max} = \sqrt{S_{max}^2 - P^2} \quad (0)$$

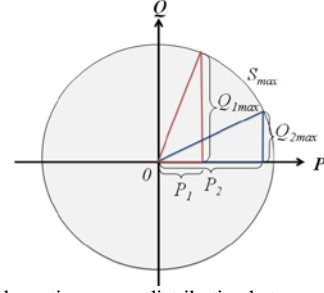


Fig. 5. Active and reactive power distribution between two units.

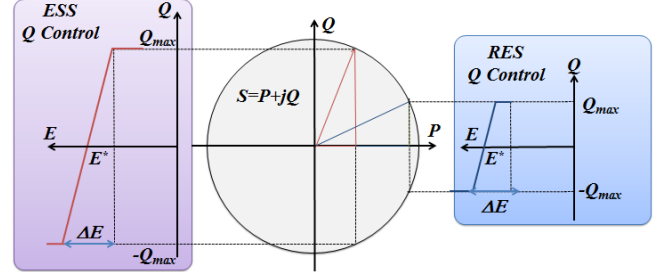


Fig. 6. Reactive power distribution for ESS and RES units.

where P is the output active power of the ESS or RES units. Therefore the remained capacity for reactive power relationship between the two units will be

$$Q_{1max} > Q_{2max}. \quad (0)$$

It indicates that the more active power one unit can supply, the less capacity remained to inject reactive power. Therefore, instead of independently controlling the reactive power with constant droop coefficients n_E and n_R in (5) and (6), coordinated reactive power control can be achieved by adaptively adjusting the master/slave droop coefficients n according to the remained reactive power capacity:

$$n = \frac{\Delta E}{\sqrt{S_{max}^2 - P^2}} \quad (0)$$

Then, based on (9), the reactive power distribution among VCM and CCM units can be deduced as

$$Q_1 : Q_2 \cdots : Q_i = \sqrt{S_{max}^2 - P_1^2} : \sqrt{S_{max}^2 - P_2^2} \cdots : \sqrt{S_{max}^2 - P_i^2} \quad (0)$$

Fig. 6 shows the reactive power distribution for ESS and RES units. In order to achieve autonomous coordinated performance, the active power regulation for ESS and RES units is based on BSM control according to SoC conditions. The reactive power sharing is achieved by master and slave droop controllers in ESS and RES units respectively, and the power distribution can be constrained by the maximum apparent power and active power consumption which is represented as the S circle in Fig. 6.

III. CONTROL IMPLEMENTATION

The overall coordinated control system is shown in Fig. 7, including ESS and RES controllers implementation. The control algorithm of each unit is further divided into primary coordinated control and inner loop control respectively. The primary control aims at controlling active and reactive power flows and also frequency and voltage regulation. Therefore, the coordinated performance is mainly obtained in this level.

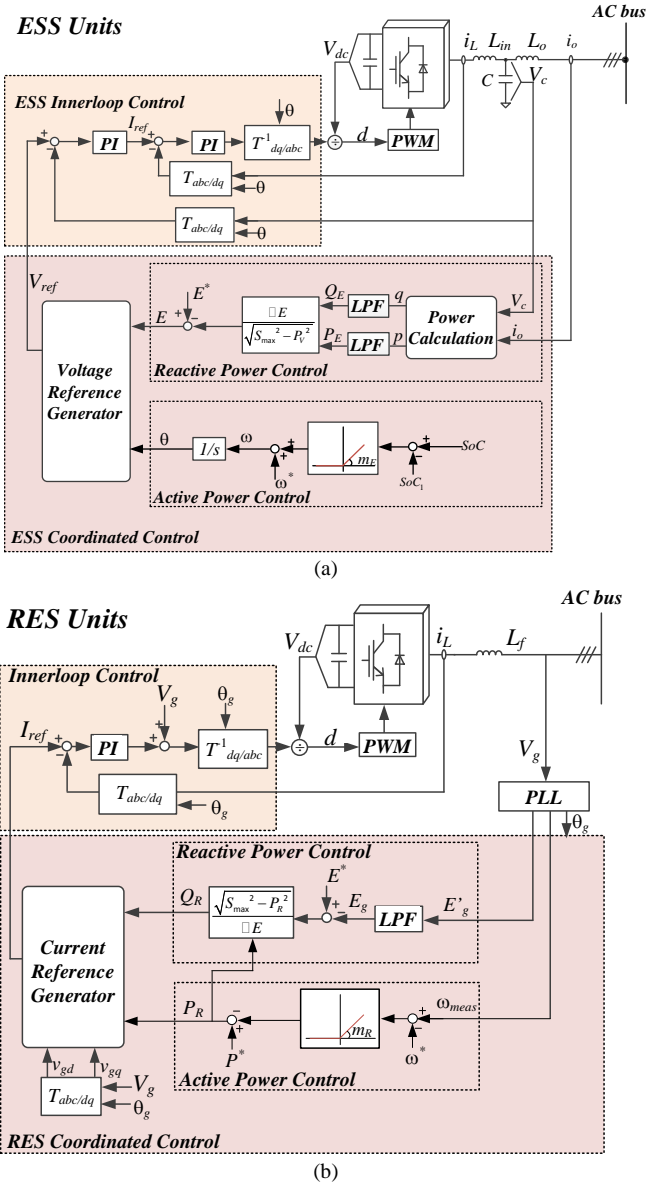


Fig. 7. Coordinated control algorithms of ESS and RES units.

After that process, the inner loop control receives the primary level commands and regulates output voltage and/or currents accordingly.

A. ESS Coordinated Control.

1) *ESS Primary Control*: Based on the previous description, the primary control of ESS is mainly divided in to active power control and reactive power control. For active power control, the ESS units execute BSM performance based on the comparison of estimated SoC and SoC_1 . Once $SoC > SoC_1$, the output frequency is increased steadily within the preset limitation according to (1) and (2). For the reactive power control, droop control (5) is adopted with the coefficient expressed in (11). The power calculation block is based on the instantaneous power theory.

2) *ESS Inner loop Control*: The inner loop control receives the voltage reference commands and regulates the capacitor voltage V_c with well know double closed loop control. The

inner loop control strategy utilizes Park transformation with PI controller in synchronous reference frame.

B. RES Coordinated Control.

1) *RES Primary Control*: The active power control utilizes slave droop control as shown in (3) and (4) when $\omega_{meas} > \omega^*$. In this way, the active power generation can be decreased so that the charging power to ESS can be limited. The slave droop shown in (6) is also utilized for reactive power regulation with coefficient defined in (11). RES units also supply reactive power proportionally to the maximum apparent power capacity. The low pass filter (LPF) used in the primary control aims at limiting the loop bandwidth, so that the primary control can be separately designed from the inner loop. The calculated active and reactive power references P_R and Q_R are sent to the current reference generator to calculate the output current reference I_{ref} .

2) *RES Inner loop Control*: After receiving the reference commands from primary control loop, the controller of RES units is used to regulate output currents with a single control loop. The control structure of inner loop is also based on synchronous reference frame with a PI controller and a grid voltage feed-forward control.

The PLL block used in RES control systems is utilized to obtain three signals: grid voltage phase θ_g , bus frequency ω_{meas} and grid side voltage amplitude E'_g . The θ_g is used in the Park and inverse Park transformations; ω_{meas} is employed in the coordinated active power control strategy, and grid side voltage amplitude E'_g is used for the coordinated control strategy. The design procedures of the PLL block can be referred in [13] to obtain these three signals.

IV. REAL-TIME HiL RESULTS

In order to validate the coordinated control strategy of ESS and RES units in islanded microgrids, hardware-in-the-loop (HiL) simulations are carried out based on dSPACE1006 platform. The simulated system consists of one ESS unit and two RES units that share common resistive and inductive loads, as shown in Fig. 8 with the parameters listed in Table I.

Fig. 9 shows the simulation results of active power coordinated control performance. In scenario S_1 , the ESS is not near to be fully charged ($SoC < 95\%$), so that bus frequency is kept at 50Hz by the ESS VCM control. RES units are generating constant power at 1.3kW and 2kW respectively. In scenario S_2 as the ESS keeps absorbing power, the SoC reaches a value above the charging threshold ($SoC > 95\%$), then the bus frequency increases to 50.25Hz. At the same time, all RES units decrease their power generation to 620W and 980W respectively to support the active power of loads. At 100s, load active power step occurs from 1.6kW to 2.4kW. In scenario S_3 , it can be seen that the ESS unit supplies the instantaneous power for the load change and the SoC starts to decrease. Due to the effect of BSM control the bus frequency also decreases correspondingly to inform the RES increases

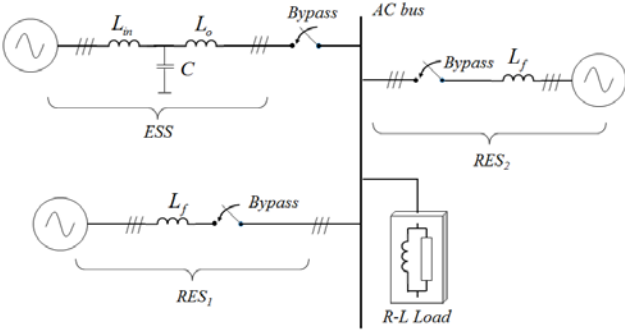


Fig. 8. Real-time HiL simulation configuration.

generation in order to compensate power increase. In steady state, the bus frequency is stable at 50.14Hz and active power generated by RES increases to 1kW and 1.45kW respectively.

Fig. 10 shows the simulation results of reactive power coordinated control performance. In scenario S_1 , both RES units are not started, so that the active and reactive power of loads is supplied by ESS unit at 1.6kW and 1.27kVar. In scenario S_2 , RES₁ starts and generates active power of 2kW. Based on the proposed coordinated reactive power control, the ESS and RES₁ share the reactive power according to the apparent power limitation at 740Var and 560Var ($Q_E : Q_{R1}=1.32:1$). In scenario S_3 , the RES₂ starts and output 1.3kW, then the reactive power distribution of ESS and both RES units change to 450Var, 390Var and 470Var ($Q_E : Q_{R1} : Q_{R2}=1.15:1:1.2$). In scenario S_4 , the reactive power of loads changes from 1.27kVar to 1.95kVar. All the distributed units increase the reactive power to supply loads and at the same time remain the same sequence as $Q_{R1} < Q_E < Q_{R2}$. Notice that there is a small difference in the reactive power outputs between the simulation results and the ideal value calculated from (12), due to the line impedance impact on the voltage and thus the reactive power sharing.

TABLE I
POWER STAGE AND CONTROL PARAMETERS

Parameter	Symbol	Value	Unit
Power Stage			
Nominal Bus Voltage	V^*	230	V
Nominal Bus Frequency	ω^*	$2\pi \cdot 50$	rad/s
Filter Inductance of ESS	L_{in}	1.8	mH
Filter Inductance of RES	L_f	3.6	mH
Filter Capacitor	C	27	μ F
Output Inductance of ESS	L_o	0.5	mH
Load	R, L	100/0.38	Ω/H
Innerloop Control			
Voltage Loop PI	k_{pV}, k_{iV}	0.1, 200	$-, s^{-1}$
Current Loop PI	k_{pI}, k_{iI}	15, 50	$-, s^{-1}$
Primary Control			
Maximum Bus frequency	ω_m	$2\pi \cdot 50.5$	rad/s
Maximum voltage deviation	ΔE	15	V
ESS Charging Threshold	SoC_1	95	%
Nominal Apparent Power	S_{max}	3	kVA

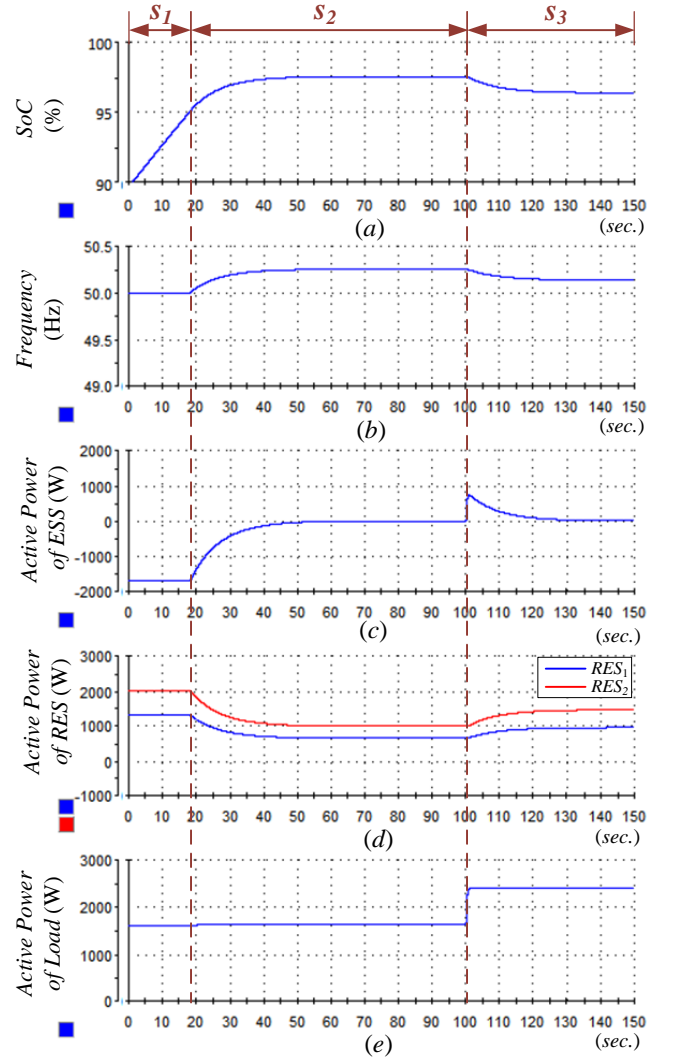


Fig. 9. Simulation results of active power coordinated control performance.

Fig. 11 shows the simulation results of active and reactive power coordinated performance. In scenario S_1 , the ESS is not in high SoC condition ($SoC < 95\%$), so that bus frequency is kept at 50Hz. The active power among ESS, RES₁ and RES₂ distribution is 1.7kW, 2kW and 1.3kW, while the reactive power distribution is 660Var, 586Var and 704Var ($Q_{R1} < Q_E < Q_{R2}$) according to (12). In scenario S_2 of $SoC > 95\%$, the RES units decreases their power generation and ESS limits the absorbed power. In the steady-state the active power distribution is 0W, 984W 640W and resulting from the active power coordinated control action. Although reactive power in loads remain the same, the reactive power among ESS, RES₁ and RES₂ is re-distributed as 665Var, 627Var and 648Var ($Q_{R1} < Q_{R2} < Q_E$), showing that the change in the active power will produce a reactive power redistribution.

V. CONCLUSION

This paper proposed a coordinated active and reactive power-sharing control among RES and ESS without using any communication system. The bus-signaling method is

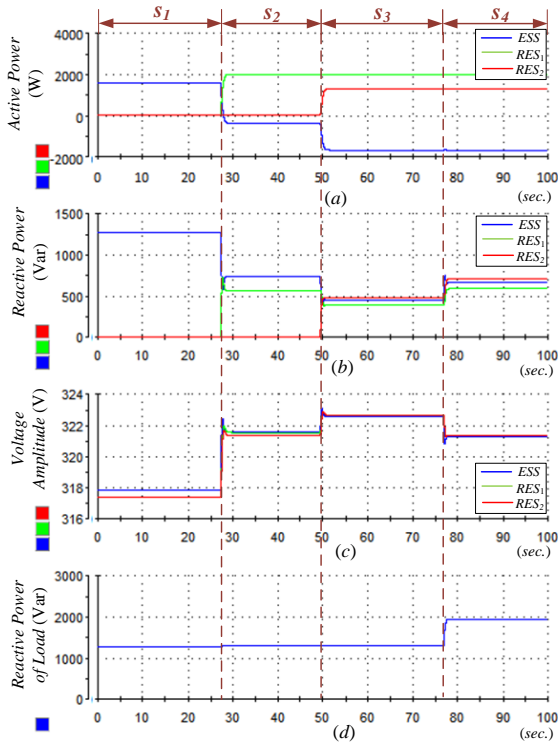


Fig. 10. Simulation results of reactive power coordinated performance.

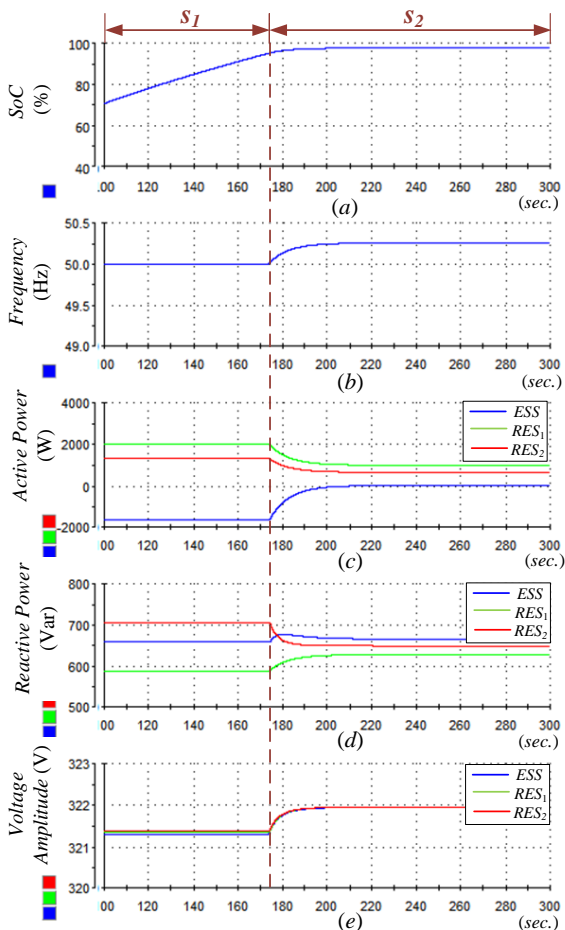


Fig. 11. Simulation results of integrated active and reactive power coordinated performance.

employed here to limit the charging power when the ESS is approaching fully charged for active power regulation. Master droop and slave droop controls that take into account the apparent power limits are implemented respectively for VCM and CCM converters for reactive power regulation purposes. Real time HiL simulation results showed the feasibility of the proposed control strategy.

In a sharp contrast to the conventional droop method, this technique is able to coordinate RES/ESS active power while providing adaptive reactive power control. Notice that this control method does not require any extra communication systems. However, although this technique does not optimize the active/reactive power flow by itself, it can act as a primary control of inside a hierarchical control structure that may operate in an emergency mode when the microgrid communication system is collapsed or damaged, thus being able to operate autonomously.

REFERENCES

- [1] J. M. Guerrero, P. C. Loh, T.-L. Lee, M. Chandorkar, "Advanced Control Architectures for Intelligent Microgrids—Part II: Power Quality, Energy Storage, and AC/DC Microgrids," *IEEE Trans. Ind. Electron.*, vol. 60, no. 4, pp.1263,1270, Apr. 2013
- [2] C. Yuen, A. Oudalov, A. Timbus, "The Provision of Frequency Control Reserves From Multiple Microgrids," *IEEE Trans. Ind. Electron.*, vol.58, no.1, pp.173,183, Jan. 2011.
- [3] J.M. Guerrero, N. Berbel, J. Matas, J. L. Sosa, and L. G. de Vicuna, "Control of line-interactive UPS connected in parallel forming a microgrid," in *Proc. IEEE ISIE*, 2007, pp. 2667–2672.
- [4] H. Kanchev, L. Di, F. Colas, V. Lazarov, B. Francois, "Energy Management and Operational Planning of a Microgrid With a PV-Based Active Generator for Smart Grid Applications," *IEEE Trans. Ind. Electron.*, vol.58, no.10, pp.4583-4592, Oct. 2011.
- [5] D. Boroyevich, I. Cvetkovic, D. Dong, R. Burgos, F. Wang, and F. Lee, "Future electronic power distribution systems a contemplative view," in *Proc. Int. Optimization of Electrical and Electronic Equipment Conf.*, 2010, pp. 1369–1380.
- [6] J. Schonbergerschonberger, R. Duke, and S. D. Round, "DC-Bus Signaling: A Distributed Control Strategy for a Hybrid Renewable Nanogrid," *IEEE Trans. Ind. Electron.*, vol. 53, no. 5, pp. 1453–1460, Oct. 2006.
- [7] D. J. Perreault, R. L. Selders, and J. G. Kassakian, "Frequency-based current-sharing techniques for paralleled power converters," *IEEE Trans. Power Electron.*, vol. 13, no. 4, pp. 626–634, Jul. 1998.
- [8] A. Tuladhar, J. Hua, T. Unger, K. Mauch, "Control of parallel inverters in distributed AC power systems with consideration of line impedance effect," *IEEE Trans. Ind. Appl.*, vol.36, no.1, pp.131,138, Jan/Feb 2000.
- [9] J. M. Guerrero, L. G. Vicuna, J. Matas, M. Castilla, and J. Miret, "A Wireless Controller to Enhance Dynamic Performance of Parallel Inverters in Distributed Generation Systems," *IEEE Trans. Power Electron.*, vol. 19, , pp. 1205–1213, Sep. 2004.
- [10] J. M. Guerrero, L. Hang, and J. Uceda, "Control of Distributed Uninterruptible Power Supply Systems," *IEEE Trans. Ind. Electron.*, vol. 55, pp. 2845–2859, Aug. 2008.
- [11] D. Wu; J. M. Guerrero, J. C. Vasquez, T. Dragicevic.; F. Tang, "Coordinated power control strategy based on primary-frequency-signaling for islanded microgrids," in *Proc. IEEE ECCE'2013*, pp.1033,1038, 15-19 Sept.
- [12] Masetti, C., "Revision of European Standard EN 50160 on power quality: Reasons and solutions," in *Proc. ICHQP 2010*, pp.1.7, 26-29.
- [13] V. Kaura, V. Blasko, "Operation of a phase locked loop system under distorted utility conditions," in *Proc. IEEE APEC '96*, pp.703,708.